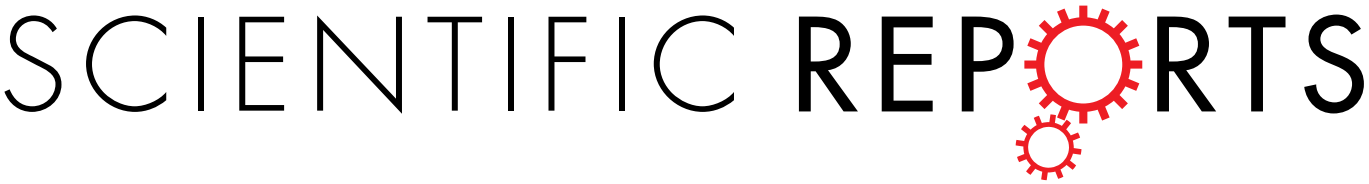

OPEN

Role of an external electric field on hybrid halide perovskite $CH_3NH_3PbI_3$ band gaps

Received: 15 January 2018
Accepted: 18 July 2018
Published online: 21 August 2018

Denghui Ji[1,2], Mula Na[3], Shuling Wang[2], Hong Zhang[2], Kun Zhu[1], CongMin Zhang[2] & Xiuling Li[4]

The organic-inorganic perovskite $CH_3NH_3PbI_3$ has attracted much attention due to their power conversion efficiency as a potential photovoltaic material, but the role of an external electric field has not been well understood. Based on first-principles calculations, the effects of an external electric field (*E*) applied along the [111] direction of the orthorhombic perovskite, $CH_3NH_3PbI_3$, on its electronic structure and optical properties are investigated. Our results indicate that the electric field strength affects the band gap (E_g) of $CH_3NH_3PbI_3$ ($MAPbI_3$, $MA = CH_3NH_3$). The energy difference between the two peaks closest to the Fermi level in the density of states diagram decreases with increasing applied electric field strength along the [111] direction, indicating that the covalent character increases between A-sites cations and I-sites anions. Both the cell volume and the final energy show the same increasing trend. The absorption peaks move toward the visible-frequency range, with the optimal band gap of 1.1–1.45 eV and $E = 0.04$–0.06 eV/Å/e. In particular, the non-linear change of the second-order Stark effect causes a non-linear change in the band gap.

The organic-inorganic hybrid perovskite $CH_3NH_3PbI_3$ has attracted much attention for its use as a photon absorber in thin-film solar cells. In addition, its synthesis is relatively straightforward and can be achieved by simple layer deposition[1–6]. Although great success has been achieved in improving the photovoltaic energy conversion efficiency of this perovskite[2,7], perovskites are ideal because they absorb most of the solar spectrum, from the ultraviolet region to the near-infrared region, generate more excitons as more photons absorbed, and bring the energy levels closer to that of the electron transport layer (ETL) or hole transport layer (HTL). The optimal band gap for a single junction solar cell is between 1.1 and 1.4 eV[8,9]. However, $CH_3NH_3PbI_3$ has a narrow direct band gap energy (E_g) of 1.51 eV, which is not optimal and hinders its application.

Using first-principles calculations, Amat *et al.*[10] investigated tetragonal $APbI_3$ perovskites with $A = Cs^+$, $(CH_3NH_3)^+$, and $(NH_2)_2CH^+$ and found that $CH_3NH_3PbI_3$ and $(NH_2)_2CHPbI_3$ have the same band gap. Hao *et al.*[11] studied the performance of $CH_3NH_3Sn_{1-x}Pb_xI_3$ perovskite solar cells. Their results indicated that the band gaps of mixed Pb/Sn hybrid perovskites have two extremes, 1.55 and 1.35 eV, depending on the ratio of Pb to Sn, but the band gaps were narrow (<1.3 eV). Furthermore, a band gap of 1.60 eV for $CH_3NH_3PbI_3$[12], 2.39 eV for $CH_3NH_3PbBr_3$, and 3.17 eV for $CH_3NH_3PbCl_3$[13,14] was obtained. Moreover, it was shown that the optical band gap can be tuned from a direct band gap of 1.52 eV to an indirect band gap of 2.64 eV by varying the CH_3NH_3I concentration[15]. In addition, the band gap of the tetragonal phase of $CH_3NH_3PbI_3$ decreased with decreasing temperature[16], following the relationship $E_g(T) = E_g(T_0) - b \cdot k_B \cdot (T_0 - T)^2$. Thus, finding the optimal band structure remains an important physical problem.

In many cases, the electric field effect can change the geometric, electronic, magnetic, and band structures of materials, and thus regulate their physical properties. Zhao *et al.*[17] reported the influence of external electric fields on the electronic structure and optical properties of TiO_2. They found that the band gap of TiO_2 becomes narrower with increasing electric field strength, decreasing to 0 eV when the electric field is 0.25 eV. Varignon *et al.*[18] used an electric field to control the Jahn-Teller distortions in bulk perovskites such as $SrTiO_3$, $BaMnO_3$,

[1]School of Electrical engineering, Liupanshui Normal University, Liupanshui City, 553004, People's Republic of China. [2]School of Mathematics and Physics, Hebei University of Engineering, Handan City, 056038, People's Republic of China. [3]Department of General Education Courses, Hebei Agricultural University Bohai Campus, Huanghua City, 061100, People's Republic of China. [4]College of Physics and Information Engineering, Hebei Advanced Thin Films Laboratory, Hebei Normal University, Shijiazhuang City, 050024, People's Republic of China. Correspondence and requests for materials should be addressed to D.J. (email: jidenghui2007@163.com)

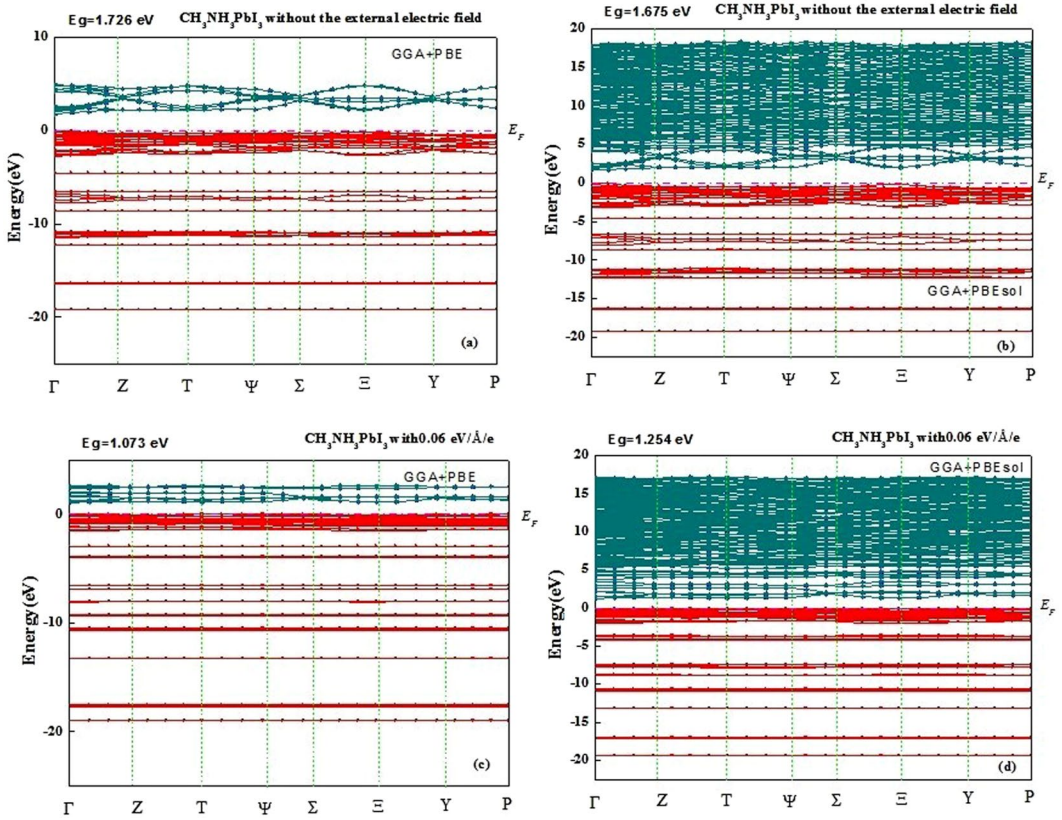

Figure 1. Band structure of $CH_3NH_3PbI_3$, calculated by GGA + PBE without the external electric field (**a**), calculated by GGA + PBEsol without the external electric field (**b**), calculated by GGA + PBE with the external electric field 0.06 eV/Å/e (**c**), and calculated by GGA + PBEsol with the external electric field 0.06 eV/Å/e (**d**).

$YMnO_3$, and $BiFeO_3$. Bellaiche *et al.* reported that an external electric field could induce polarization paths in $PbZr_{1-x}Ti_xO_3$ perovskites and lead to the expected sequence of tetragonal, A-type monoclinic, and rhombohedral structures[19]. Xu *et al.*[20] demonstrated that electric fields could induce a change from a ferroelectric phase to an antiferroelectric phase in a lead-free $NaNbO_3$-based polycrystalline ceramic. Therefore, it is very important and valuable to investigate the relationship between external electric fields and the physical properties of the organic-inorganic hybrid perovskite $CH_3NH_3PbI_3$. $CH_3NH_3PbI_3$ undergoes two phase transitions, one at 160 K (orthorhombic to tetragonal) and the other at 330 K (tetragonal to cubic)[21]. Using Density functional theory (DFT) calculations, Leppert *et al.* investigated the Rashba effect induced by the electric field and strained in the hybrid halide perovskite $CH_3NH_3PbI_3$ with a tetragonal and cubic structure[22]. Although the orthorhombic phase is realized with rotations about the C–N axis that freeze out when $T \leq 162$ K, temperature is not the only factor affecting these properties. An external electric field or magnetic field could also be an important factor, so we chose the orthorhombic $CH_3NH_3PbI_3$ as our subject to investigate these effects.

In this article, we investigate the effects of an external electric field applied along the [111] direction on the geometry structure, electronic energy band structure, total density of states, and optical properties of $CH_3NH_3PbI_3$. This study provides a method for obtaining the optimal band gap of $CH_3NH_3PbI_3$ and expands the scope of its applications.

Results and Discussion

The effects of the external electric field (E) direction, including the [001], [010], [100], [110], and [111] directions, on the band structure of $CH_3NH_3PbI_3$ were studied. The application of an electric field along the [111] direction in $CH_3NH_3PbI_3$ decreases the band gap, while fields aligned along the other directions increase the band gap. Therefore, we only investigated the physical properties of $CH_3NH_3PbI_3$ under an electric field aligned along the [111] direction to obtain the optimal band gap of 1.1–1.4 eV.

Band structure of $CH_3NH_3PbI_3$ under the external electric field. The band structure of $CH_3NH_3PbI_3$ in the absence of an external electric field is shown in Fig. 1 (a,b). When the external electric field is equal to zero, the valence band maximum (VBM) and the conduction band minimum (CBM) are located at the same Γ-point, which indicates that $CH_3NH_3PbI_3$ possesses direct semiconductor characteristics. The calculated band is 1.726 eV and 1.675 eV, corresponding to the generalized gradient approximation (GGA) functional developed by Perdew, Burke, and Ernzerhof PBE[23] and PBEsol[24], which are similar to the results[25] reported by Menéndez-Proupin *et al.* The detailed calculation methods were shown in the Method section. It should be noted that the number

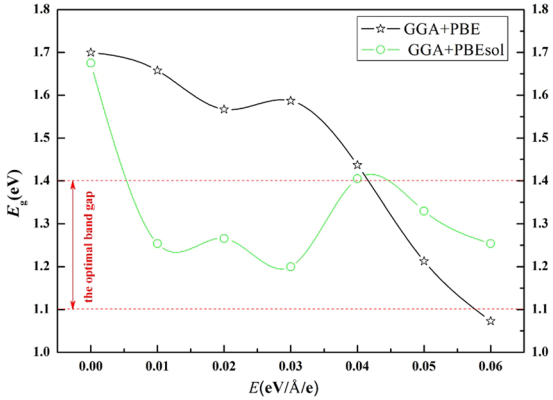

Figure 2. The curves of band gap (E_g) versus the external electric field (E) of $CH_3NH_3PbI_3$ perovskite calculated by GGA + PBE and GGA + PBEsol.

of conduction bands calculated using GGA + PBEsol is greater than that calculated using GGA + PBE. In the presence of an applied external electric field with a strength ranging from 0.01 to 0.06 eV/Å/e, the band structures of the orthorhombic $CH_3NH_3PbI_3$ are similar. Figure 1 (c,d) show the band structure when $E = 0.06$ eV/Å/e. The conduction band shifts downward to the Fermi level (0 eV) and the energy band near the CBM is more dispersed, resulting in a change in the band gaps. All the configurations indicate an indirect band gap semiconductor, and the VBM and CBM are located at the centre of the Γ-point in k space. Because of the narrower indirect band gap of the $CH_3NH_3PbI_3$ semiconductor, only a small amount of energy is required for the formation of excitons. However, the GGA + PBE and GGA + PBEsol methods underestimate the band gap because of self-interaction errors, suggesting that the actual band gap of $CH_3NH_3PbI_3$ is slightly smaller than the calculated values.

The band gaps of $CH_3NH_3PbI_3$ are strongly affected by the applied electrical field strength. As the external electric field strength increases, the band gaps calculated by GGA + PBE first decrease linearly, then increase slightly, and finally, decrease linearly. The band gaps calculated by GGA + PBEsol indicated the optimal value between 1.1 and 1.4 eV for all the structures under an external electric field, as shown in Fig. 2. Therefore, both the results indicated that the external electric field contributes to a decrease in the band gap.

Density of states of $CH_3NH_3PbI_3$ under an external electric field. Figure 3 (a) calculated by GGA + PBE and (b) calculated by GGA + PBEsol show the total density of states (TDOS) of $CH_3NH_3PbI_3$ in the presence of an external electric field ($E = 0.00$–0.06 eV/Å/e). As the external electric field increases, (i) the two peaks corresponding to orbital energies from −22.5 to −15 eV gradually broaden and then become narrow, reaching their maximum widths when $E = 0.03$ eV/Å/e. (ii) The five peaks corresponding to orbital energies between −15 and −5.5 eV gradually broaden. (iii) Parts of the TDOS of the orbitals crossing the Fermi level increase with increasing external electric field, suggesting that the band gap of $CH_3NH_3PbI_3$ decreases. (iv) The CBM gradually narrows and shifts to the Fermi level, which also decreases the band gap, suggesting a pseudo-energy gap decrease, while the strength of the covalent character increases between the MA-cations and I anions.

The electron densities of $CH_3NH_3PbI_3$ when $E = 0.00$ and 0.06 eV/Å/e were shown in Fig. 4 (a,b), calculated by GGA + PBEsol. It can be seen that: (i) the lost electronic ions are H and Pb cations, and the gain electronic ions are C, N and I anions. (ii) With increasing external electric field, the electron density of C-N increases, thus increasing the strength of the associated covalent bond. (iii) The exact value of gain or lost electrons can be obtained based on Milliken Charge Analysis Method of Wave Function. For the $E = 0.00$, the lost average H cations have three kinds including 0.34, 0.22, and 0.21 electrons, the lost average Pb cations have one kind with 0.88 electrons, the gain anions with C and N have 0.61 and 0.70 electrons, and the gain I anion have two kinds including 0.36 and 0.52 electrons. For the $E = 0.06$ eV/Å/e, the lost average H cations have seven kinds including 0.15, 0.16, 0.29, 0.30, 0.34, 0.35 and 0.44 electrons, the lost average Pb cations have one kind with 0.54 electrons, the gain C anions have 0.65 electrons, the gain N anions have two kinds including 0.77 and 0.76 electrons, and the gain I anion have six kinds including 0.29, 0.37, 0.38, 0.39, 0.40, and 0.41 electrons.

Figure 5 shows the partial density of states (PDOS) of $CH_3NH_3PbI_3$ (GGA + PBEsol) under applied external electric field strengths of $E = 0.00$ and 0.06 eV/Å/e. The electronic orbitals 5d6s6p, 5s5p, 2s2p, 2s2p, and 1s are modeled as the valence orbitals for Pb, I, C, N, and H, respectively. The s-p hybrid level increases with external electric field increasing, and the effect on the conduction band is much more pronounced than that on the valance band. The peak near the orbital energy level at −5.0 eV splits into two peaks, which is attributed to the Stark effect of the s and p electrons, and one peak position shifts to the Fermi level. The external electric field causes the d electrons of Pb to shift to higher energies, but the d electrons do not affect the s and p electrons.

The Stark effect can induce the splitting of degenerate energy levels. The degree of the band splitting increases with the electric field, and a smaller band gap can be obtained. All peaks of the orbital energy level in the DOS curves broaden and shift to lower energies as E increases. The physical mechanisms underlying the change in the band structure of $CH_3NH_3PbI_3$ is ascribed to the C-N and Pb-I bond lengths, changes in the lattice structure, and charge transfer between the Pb and I atoms. The lattice distortion caused by the mutation of lattice parameters may lead to change in the microscopic electric structure, band structure, and density of states, similar to the results reported in ref.[17].

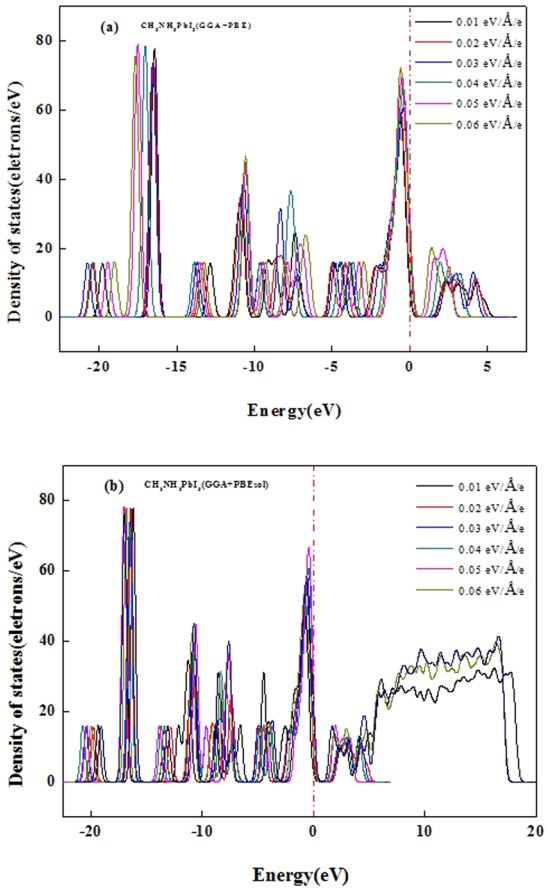

Figure 3. The total density of states (TDOS) of $CH_3NH_3PbI_3$ calculated by GGA + PBE or GGA + PBEsol with the external electric field $E = 0.00–0.06$ eV/Å/e.

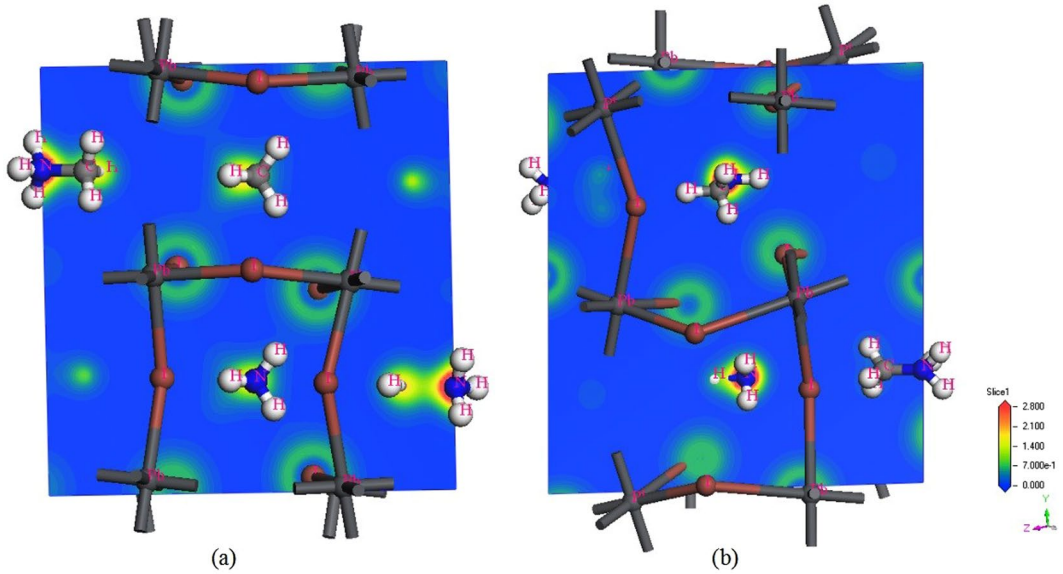

Figure 4. The electron density of $CH_3NH_3PbI_3$ calculated by GGA + PBEsol with the external electric field 0.00 eV/Å/e (**a**), and 0.06 eV/Å/e (**b**).

Optimized structure of $CH_3NH_3PbI_3$ under an external electric field. The crystal structure determines the physical properties of the material; the lattice parameters (*a*, *b*, and *c*), cell volume (*V*), bond length (*d*), and final energies (E_{Final}) are listed in Table 1. The external electric field applied along the [111] direction stretches

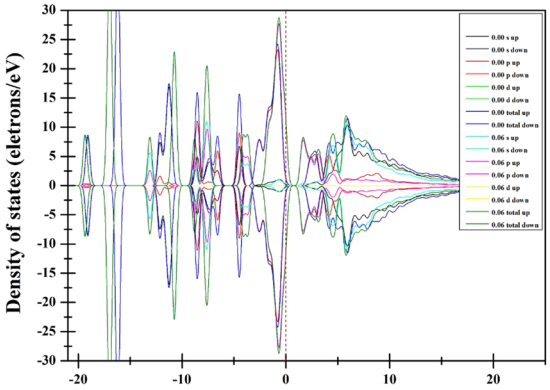

Figure 5. The partial-total density of states (PDOS) of $CH_3NH_3PbI_3$ (GGA + PBEsol) with the external electric field $E = 0.00$ and 0.06 eV/Å/e.

the lattice parameters. Figure 6 shows that both the final energies and the cell volumes increase monotonically, and the final energies obtained by GGA + PBE are lower than those obtained by GGA + PBEsol. The GGA + PBE results follow the fitted relationships $E_{\text{Final}}(E) = 1591.989E - 12504.565$ and $V(E) = 1035.804E + 983.666$. In addition, the bond distances, including the d(C-N) and d(I-Pb) distances, increase monotonously with increasing E, which leads to weak interactions between C and N as well as between I and Pb. To illustrate the extent of lattice distortion, two parameters ($n_1 = \frac{b/\sqrt{2} - a}{a}$, and $n_2 = \frac{b/\sqrt{2} - c}{c}$) can be used for describing the degree of deviation from the cubic structure[26]. The curves for these parameters *versus* the external electric field are shown in Fig. 7. For the results based on the GGA + PBE or GGA + PBEsol method, both n_1 and n_2 are positive, suggesting that the orthogonal structures are of the O type, where $\frac{c}{\sqrt{2}} > b$, $\frac{a}{\sqrt{2}} > b$, and the deviations range from 2.31% to 27.86%, which are much greater than those for single inorganic perovskites[27].

In addition, the orientation of the $CH_3NH_3^+$ ion can be seen in the orthogonal $CH_3NH_3PbI_3$. Table 1 shows the Cartesian coordinates of the C and N atoms are displaced by 0.01 Å along the [111] direction, which is similar to a past report that Pb and apical I atoms are displaced by 0.1 Å and 0.01 Å along the [001] direction in P4mm $CH_3NH_3PbI_3$ (ref.[22]). The Pb-N-C angle decreases with increasing external electric field, which consistents with the increase in the lattice parameters and cell volume.

Optical properties of $CH_3NH_3PbI_3$ under an external electric field. $CH_3NH_3PbI_3$ may show different preferential growth directions with different substrates, so obtaining the optical performance in this growth direction is an important physical problem. Let us take the [100] direction as the preferred growth direction as an example to illustrate this problem. Figure 8 (a) calculated by GGA + PBE and (b) calculated by GGA + PBEsol show the optical absorption spectrum with polarized light, where the polarization is along the [100] direction of $CH_3NH_3PbI_3$ in the presence of an external electric field. It is seen that the electric field significantly influences the optical absorption characteristics of $CH_3NH_3PbI_3$. We assume the highest intensity absorption peak as the main absorption peak. The values 5.5 eV and 3.68 eV in the range of 0~5 eV for $CH_3NH_3PbI_3$ calculated by the GGA + PBE and GGA + PBEsol methods are the positions of the main absorption peak without the external electric field, which corresponds to absorbed light with the highest frequency. As the external electric field increases, the peak positions shift to lower frequencies, approaching the visible light region, and full width at half maximum (FWHM) of the absorption peaks decreases, which makes light absorption more effective and thus improves the photoelectric conversion. In addition, there are some absorption peaks at higher energies beyond the visible range, which do not play a major role in photoelectric conversion, but can become a candidate as optical detection device such as ultraviolet band.

As the first-order approximation, the band gap E_g and wavelength should satisfy the following relation:

$$\lambda(\text{nm}) = 1239.8/E_g(\text{eV}). \quad (1)$$

We can obtain the related data based on eq. 1, as shown in Table 2. The following can be deduced:

(i) The band gap decreases non-linearly with increasing external electric field. When $E \leq 0.03$ eV/Å/e, ν *and* ν_{100} decrease with an increase in the external electric field; when $E \geq 0.04$ eV/Å/e, ν *and* ν_{100} increase with external electric field increasing, except ν with 0.04 eV/Å/e based on the GGA + PBE. Here, ν is the frequency calculated by the band gap, ν_{100} is the frequency along the [100] direction based on the Fig. 8.

(ii) The band gap (*Eg*) based on the band structure is similar to E_g' based on the optical properties. Based on adiabatic approximation and single electron approximation, the relationship between absorption coefficient and photon energy can be expressed as,

$$\alpha = B(h\nu - E'_g), \quad (2)$$

Functions	Optimized structure	$x=0.00$	$x=0.01$	$x=0.02$	$x=0.03$	$x=0.04$	$x=0.05$	$x=0.06$
PBE	a	8.9032	9.2071	9.2584	9.2498	9.3200	9.2692	9.0738
	b	13.0752	13.9164	14.4428	14.9694	15.2694	15.5758	16.0369
	c	8.4972	8.6082	8.7385	9.0650	10.0066	10.6834	10.8378
	V	989.1600	1102.9588	1168.4963	1255.1677	1424.0542	1542.4216	1577.0738
	d(C-N)	1.493	1.488	1.490	1.493	1.496	1.500	1.502
	d(I-Pb)	3.169	3.273	3.430	3.538	3.690	3.773	4.318
		3.320	3.539	3.634	3.761	3.874	4.012	4.144
	E_{Final}	−12501.21889	−12489.29171	−12475.24448	−12459.64554	−12441.06694	−12422.84539	−12408.32328
	Cartesian coordinates (x,y,z)							
	Pb	(0,0,0.5)	(0,0,0.5)	(0,0,0.5)	(0,0,0.5)	(0,0,0.5)	(0,0,0.5)	(0,0,0.5)
	C	(0.0876,0,75, 0.9447)	(0.0866,0.75, 0.9556)	(0.0932,0.75, 0.9159)	(0.0994,0.75, 0.9211)	(0.0994,0.75, 0.9211)	(0.1094,0.75, 0.9107)	(0.1152,0.75, 0.9041)
	N	(−0.0585, 0.75, 1.0185)	(−0.0651, 0.75, 1.013)	(−0.0493, 0.75, 1.0065)	(−0.0429, 0.75, 0.9990)	(−0.0429, 0.75, 0.9890)	(−0.0285, 0.75, 0.9843)	(−0.0229, 0.75, 0.9797)
	θ	77.005	78.465	76.549	78.138	77.338	76.718	76.674
PBEsol	a	8.8774	8.9074	8.8567	8.7382	8.6475	8.4017	8.2677
	b	12.8425	13.3065	13.4663	13.8718	14.16068	14.4834	14.9474
	c	8.5542	8.4694	8.5846	8.8155	9.2884	9.9500	10.3411
	V	975.2591	1003.8505	1023.8576	1068.5584	1137.4005	1210.7628	1277.9559
	d(C-N)	1.481	1.479	1.481	1.482	1.482	1.479	1.472
	d(I-Pb)	3.201	3.388	3.413	3.492	3.578	3.700	3.856
		3.299	2.952	3.004	2.990	3.513	3.545	3.350
	E_{Final}	−12458.46453	−12449.90457	−12449.90457	−12437.68499	−12424.7522	−12411.71698	−12397.74163
	Cartesian coordinates (x,y,z)							
	Pb	(0,0,0.5)	(0,0,0.5)	(0,0,0.5)	(0,0,0.5)	(0,0,0.5)	(0,0,0.5)	(0,0,0.5)
	C	(0.0905,0,75, 0.9352)	(0.0947,0.75, 0.9333)	(0.0968,0.75, 0.9226)	(0.1019,0.75, 0.9160)	(0.1049,0.75, 0.9130)	(0.1100,0.75, 0.9072)	(0.1142,0.75, 0.8987)
	N	(−0.0600, 0.75, 1.0093)	(−0.0549, 0.75, 1.0089)	(−0.0484, 0.75, 1.0080)	(−0.0406, 0.75, 1.0073)	(−0.0351, 0.75, 1.0050)	(−0.0246, 0.75, 1.0029)	(−0.0147, 0.75, 0.9969)
	θ	77.112	77.752	76.698	76.081	75.260	73.583	72.869

Table 1. Optimized structure of $CH_3NH_3PbI_3$ with the external electric field $E=0.00$–0.06 eV/Å/e including lattice parameters (a, b, c), bond distances (d), cell volumes (V), the final energies (E_{Final}), Cartesian coordinates of Pb, C, and N, and the Pb-N-C angle. Units are Å, Å, Å^3, eV, 1, and °.

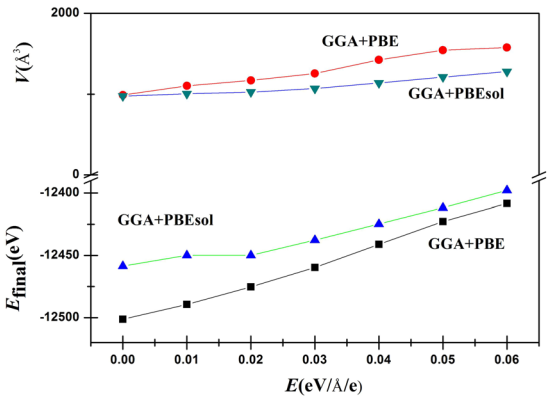

Figure 6. The curve of the final energy (E_{final}) and cell volumes (V) increases with the external electric field E.

where a is the absorption coefficient, B is a fitting parameter, h is Planck's constant, ν is frequency, and E_g' is the band gap. According to the data in Fig. 8, E_g' values based on the optic properties are shown in Table 2.

Moreover, although the preferred growth direction may be not [100] in practice, we provided a method to obtain the optical properties of $CH_3NH_3PbI_3$ under an external electric field.

Why does the band gap decrease non-linearly? For $CH_3NH_3PbI_3$ under an external electric field, the Hamiltonian can be written as,

$$\hat{H} = \hat{H}_0 + \hat{H}', \tag{3}$$

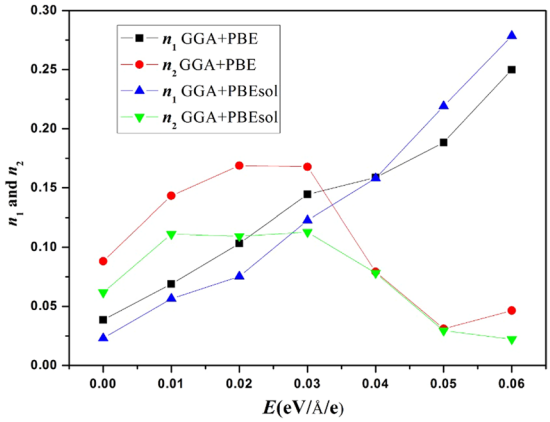

Figure 7. Parameters n_1 and n_2 *versus* the external electric field E. Here $n_1 = \frac{b/\sqrt{2} - a}{a}$, and $n_2 = \frac{b/\sqrt{2} - c}{c}$.

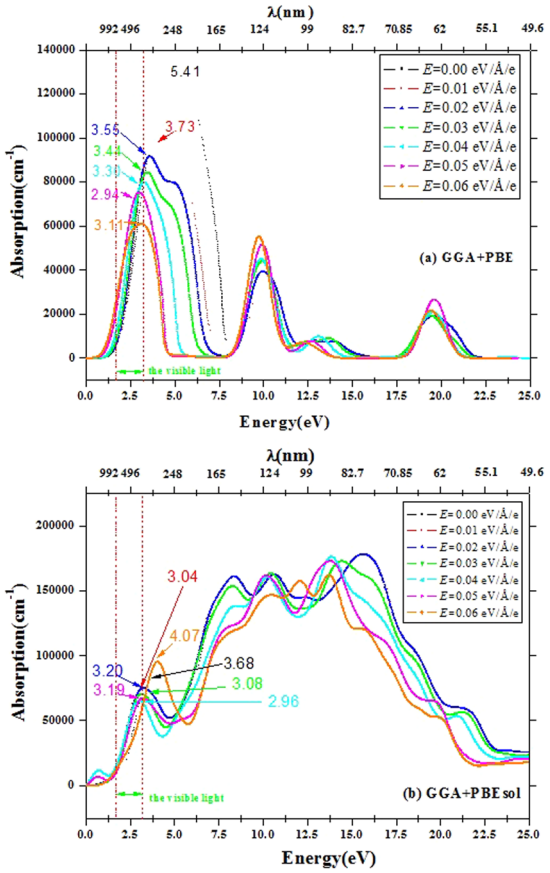

Figure 8. The optical absorption spectrum within the polarized with polarization (1, 0, 0) for $CH_3NH_3PbI_3$ with the external electric field $E = 0.00$–0.06 eV/Å/e.

Here, $\hat{H}_0 = -\frac{\hbar^2}{2m}\nabla^2 + V(r)$; $\hat{H}' = e\overrightarrow{E}\cdot\overrightarrow{r} = eEr\cos\theta$; $e = 1.6 \times 10^{-19}$C; E is the external electric field; and θ is the angle between the direction of the electric field and the radius vector direction $\overrightarrow{r}$. $\hat{H}'$ is the perturbation. Based on the perturbation theory, the energy levels (E_i) will change to the initial values ($E^{(0)}{}_i$) by an amount ΔE_i.

$$E_i = E^{(0)}{}_i + \Delta E_i, \tag{4}$$

ΔE_i can be expanded with the additional energy of the electric field, which are Stark effect orders denoted as first order $\Delta E^{(1)}{}_i$ or second order $\Delta E^{(2)}{}_i$.

Functions	E (eV/Å/e)	E_g (eV)	λ (nm)	ν (10^8MHz)	ν_{100} (eV)	E_g' (eV)
GGA + PBE	0.00	1.700	729.29412	4.11357	5.41	1.72
	0.01	1.658	747.7684	4.01194	3.73	1.63
	0.02	1.567	791.19336	3.79174	3.55	1.55
	0.03	1.587	781.22243	3.84014	3.44	1.57
	0.04	1.437	862.76966	3.47717	2.30	1.43
	0.05	1.213	1022.09398	2.93515	2.94	1.20
	0.06	1.073	1155.452	2.59639	3.11	1.06
GGA + PBEsol	0.00	1.675	740.1791	4.05307	3.68	1.68
	0.01	1.254	988.67624	3.03436	3.04	1.25
	0.02	1.266	979.3049	3.0634	3.20	1.24
	0.03	1.200	1033.16667	2.90369	3.08	1.19
	0.04	1.405	882.41993	3.39974	2.96	1.40
	0.05	1.330	932.18045	3.21826	3.19	1.34
	0.06	1.254	988.67624	3.03436	4.07	1.25

Table 2. Related data obtained using eq (1). Here, E is the external electric field, E_g is the band gap based on the band structure, λ is the wavelength, ν is the frequency calculated by the band gap, ν_{100} is the frequency along the [100] direction based on the Fig. 8, and E_g' is the band gap based on the optical properties.

$$\Delta E = \Delta E^{(1)} + \Delta E^{(2)} + \cdots, \tag{5}$$

The energy changes owing to the electric field, where $<\psi_i|$ is the initial state of the system, then we have,

$$\Delta E^{(1)} = \langle\psi_i|-e\overrightarrow{E}\cdot\overrightarrow{r}|\psi_i\rangle = \langle\psi_i|-eEr\cos\theta|\psi_i\rangle, \tag{6}$$

For second-order energy changes, the summation is over all possible states of the system, so,

$$\Delta E^{(2)} = \sum_{allstates_k} \frac{\langle\psi_i|-e\overrightarrow{E}\cdot\overrightarrow{r}|\psi_k\rangle\langle\psi_k|-e\overrightarrow{E}\cdot\overrightarrow{r}|\psi_i\rangle}{E^{(0)}{}_i - E^{(0)}{}_k}, \tag{7}$$

If E can be considered a constant over the perturbation volume,

$$\Delta E^{(1)} = -e\overrightarrow{E}\langle\psi_i|\overrightarrow{r}|\psi_i\rangle, \tag{8}$$

$$\Delta E^{(2)} = \overrightarrow{E}\cdot\sum_{allstates_k} \frac{\langle\psi_i|-e\overrightarrow{r}|\psi_k\rangle\langle\psi_k|-e\overrightarrow{r}|\psi_i\rangle}{E^{(0)}{}_i - E^{(0)}{}_k}\cdot\overrightarrow{E}. \tag{9}$$

From Table 1, it can be seen that the movements of the I^- anions are coupled to the movements of the monovalent MA^+ cations and the rotation of the MA dipoles. This change in polarizability in the domains can influence the second-order Stark effect through the change in the dielectric constant owing to the change in the optical absorption spectrum[28]. Then, $\Delta E^{(2)}$ may reflect in two possible first-order Stark effects, as shown in Fig. 9. If the value of $\Delta E^{(2)}$ is positive, the band gap will widen; if the value of $\Delta E^{(2)}$ is negative, the band gap will shrink. However, the second-order Stark effect cannot be larger than the first-order Stark effect, so $CH_3NH_3PbI_3$ without an external electric field has the maximum band gap. The non-linear extent of the second-order Stark effect cause a non-linear change in the band gap.

The device required that: (i) The Highest Occupied Molecular Orbital (HOMO) of TiO_2 as ETL layer must be lower than CBM of perovskite active layer. (ii) The Lowest Unoccupied Molecular Orbital (LUMO) of spiro-omeTAD as HTL layer must be higher than VBM of perovskite active layer. The external electric field induced the Stark effect, splitting energy levels for TiO_2 and spiro-omeTAD (shown in Fig. 10), which decreases the HOMO of TiO_2 and increases the LUMO of spiro-omeTAD.

How to obtain the external electric field in practice? As a preliminary exploration, we believe that this study is valuable. Indeed, the calculated results are aimed for the orthorhombic structure and not the tetragonal structure at room temperature, but the orthorhombic $MAPbI_3$ structure can be applied to solar panels in space with lower temperature. Due to cosmic microwave background with 3 K[29], the perovskite solar cells with orthorhombic phase can accomplish as Power generation device candidate in space such as International Space Station, satellite, space shuttle, spacecraft, lunar rover vehicle, etc. Moreover, this may provide a new idea to control the properties of the tetragonal structure at room temperature.

The main reason for the orthorhombic to tetragonal transition in $CH_3NH_3PbI_3$ is temperature, and the external electric field causes the Stark effect splitting energy level of C, N, H, Pb and I, and the two structures with the same element and the similar chemical bond characters. Thus, we inferred that the Stark effect for $CH_3NH_3PbI_3$ with a tetragonal structure may be observed at room temperature.

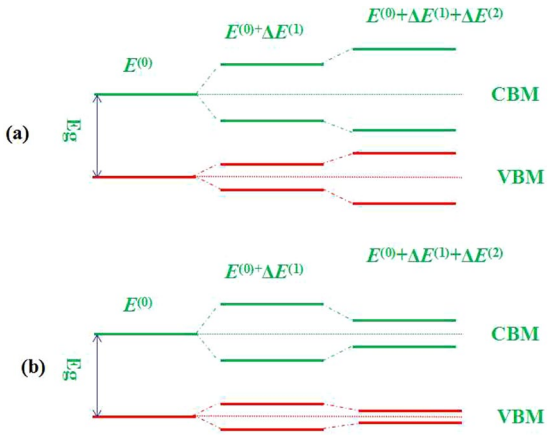

Figure 9. Schematic of the Stark effects on the band gap (E_g) process, (**a**)$\Delta E^{(2)} > 0$ and (**b**) $\Delta E^{(2)} < 0$.

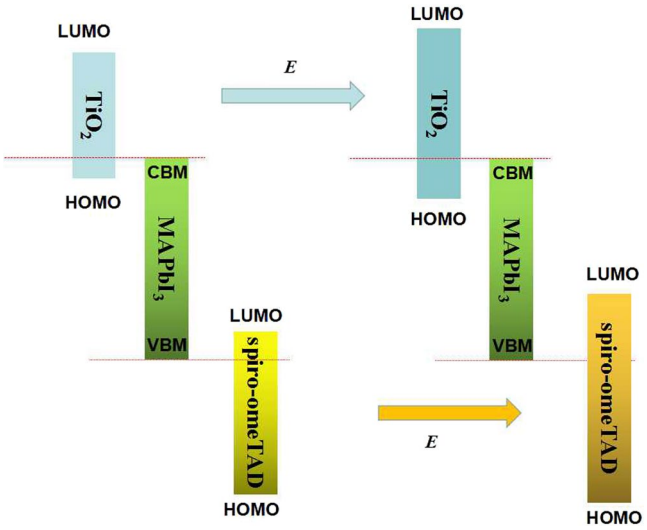

Figure 10. Schematic of external electric field on the LUMO and HOMO of TiO_2 and spiro-omeTAD process.

The device for realizing the external electric field is shown in Fig. 11, which is similar to the ref. reported by Li *et al.*[30]. It noted that the device in this study only provide the external electric field, do not provide electrons. The large DC voltage near 100 V can be obtained by DC boost circuit, which can resolve the electric field strength. The positive electrode is connected with the transparent ITO for visible light, and the negative electrode is connected with Au; the directions of the two electrodes can control the direction of the electric field, including the [111] direction. Moreover, the distance between the positive and negative electrodes, as well as the insulation thickness and dielectric constant, influenced the electric field strength.

It noted that the external electric field of about 0.06 eV/Å/e is large, which is equal to 0.6 V/nm, but this external electric field can be carried out in practice. For example, Hsu *et al*. used an external magnetic field to adjust the relative energy levels between a skyrmion and a ferromagnet globally, and obtained an electric field of 1 V/nm, which corresponds to a magnetic field of about 40 mT for their system[31]. Qin *et al*. applied an external electric field to drive the ultra-low thermal conductivity of silicene. Using an electric field ($E_z = 5$ V/nm), the lattice thermal conductivity of silicene can be reduce a record low value of 0.091 $Wm^{-1} K^{-1}$, which is comparable to that of the best thermal insulation materials[32]. The main problem caused by the huge electric field may be the device breakdown, which is attributed to the self-sustainable discharge for uniform electric field. The more uniform the electric field is, the higher the self-sustainable discharge voltage is. So the transparent ITO as the positive electrode and the Au film as the negative electrode should possess the rule shapes and flat surfaces, which would decrease the degree of dielectric polarization, and reduce the possibility of the tip discharge.

Conclusion

In conclusion, we have used first-principles calculations to calculate the geometries, band structure, electronic properties, and optical absorption properties of perovskite $CH_3NH_3PbI_3$ under an external electric field aligned along the [111] direction. The external electric field increases the lattice parameters and the cell volume, stretching the *c*-axis and influencing the degree of lattice distortion. The external electric field controls the band gap

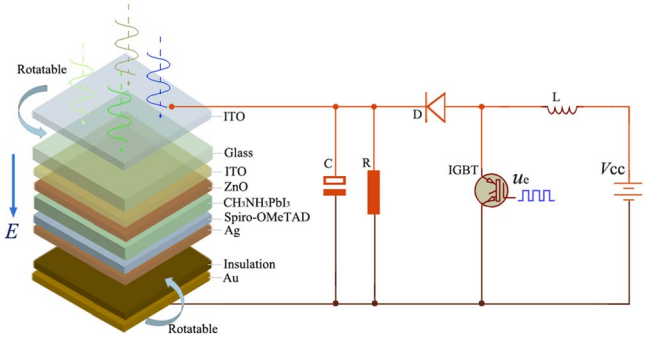

Figure 11. Device for realizing an external electric field. Here, V_{CC} is input voltage obtained by the storage battery charged by the solar battery, L is inductance, u_e is rectangular square wave pulse signal which control the duty cycle and regulate magnification, IGBT is crystal oscillator, D is diode, R is resistance, and C is capacitance.

Fractional coordinates			
Pb	0.00000	0.00000	0.50000
I	0.98041	0.25000	0.56319
I	0.18148	0.01821	0.17644
C	0.40839	0.25000	0.43168
N	0.55516	0.25000	0.51975
H	0.11881	0.31686	0.01029
H	0.15523	0.82116	0.96378
H	0.03804	0.25000	0.85812
H	0.93323	0.25000	0.19489

Table 3. The orthorhombic structure of $CH_3NH_3PbI_3$ reported by Menéndez-Proupin *et al.*[25]. Space group 62 (Pnma). Lattice parameters: $a = 8.8273$ Å, $b = 12.6793$ Å, $c = 8.5099$ Å.

from 1.70 to 1.073 eV, corresponding to external electric field strengths of 0.00 to 0.06 eV/Å/e. The rotation of the MA dipoles induced a second-order Stark effect, and the non-linear change in the second-order Stark effect causes a non-linear change in the band gap. In addition, the absorption peaks and the peak locations are affected by the external electric field. Thus, this study provides a possible method to improve the photoelectric conversion of perovskite solar cells.

Methods

$CH_3NH_3PbI_3$ perovskite undergoes two phase transitions, one at 160 K (orthorhombic to tetragonal) and the other at 330 K (tetragonal to cubic). The orthorhombic $CH_3NH_3PbI_3$ structure could be closer to that at the 0 K, so we chose this as the research object given the DFT calculations are performed at 0 K. Based on the structure reported by Menéndez-Proupin *et al.*[25], $CH_3NH_3PbI_3$ perovskite has an orthorhombic crystal structure in the space group *Pnma* (no. 62), with lattice parameters of $a = 8.8273$ Å, $b = 12.6793$ Å, and $c = 8.5099$ Å, as shown in Table 3 and Fig. 12. $CH_3NH_3PbI_3$ has a typical AMX_3 perovskite structure with the unit cell consisting of a central lead atom octahedrally coordinated to six iodide atoms. The PbI_6 octahedron is located inside a cube with each iodide at the centre of a cubic face, and the CH_3NH_3 cations are positioned at the corners of the cube. To study the effect of the electric field on the physical properties of $CH_3NH_3PbI_3$, the external electric field along different directions (x, y, and z) was investigated.

We calculated the physical properties including the energy band, the density of states (DOS), and optical absorption in the orthorhombic perovskite $CH_3NH_3PbI_3$ exposed to different external electric fields using the Cambridge Serial Total Energy Package (CASTEP)[33,34] program. The generalized gradient approximation (GGA) functional developed by Perdew, Burke, and Ernzerhof (1996, 2008, PBE, and PBEsol)[23,24] was used. These exchange-correlation functionals employed were same as those in the study of the self-regulation mechanism for charged point defects in hybrid halide perovskites reported by Walsh *et al.*[35]. The spin-orbit coupling (SOC) effect is reported to have little influence on the geometric structures[36]. Ultra-soft pseudopotentials with a cutoff energy of 310 eV (based on test results) were used to describe the interactions between the valence electrons and the ionic core, and including relativistic effects for Pb and I atoms. A $3 \times 2 \times 3$ Monkhorst-Pack k-point scheme was used to calculate the absorption spectra. We performed the convergence test, and found the results with 500 eV cutoff energy and $5 \times 5 \times 5$ Monkhorst-Pack k-point scheme to be similar to those with the above parameters. The convergence tolerances for geometry optimization calculations were set to a maximum displacement of 5.0×10^{-4} Å, maximum force of 0.01 eV/Å, maximum energy change of 5.0×10^{-6} eV/atom, maximum stress of 0.02 GPa.

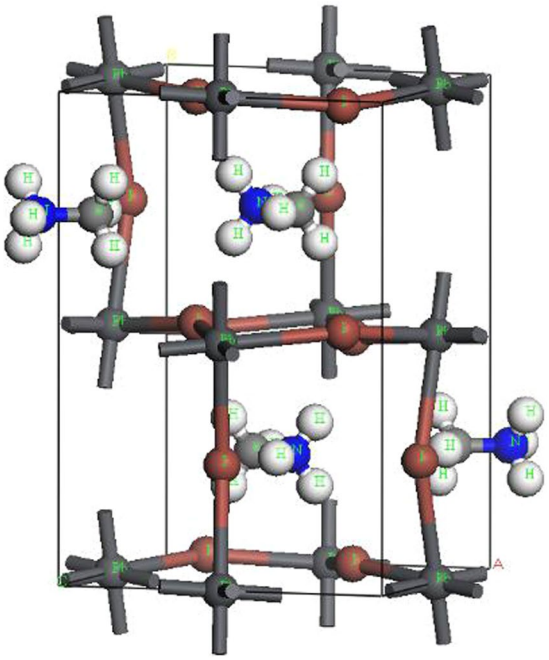

Figure 12. Unit cell of the orthorhombic $CH_3NH_3PbI_3$ perovskite.Here, white, black, blue, gray, and brown balls are H, Pb, N, C and I atoms, respectively.

According to the refs[24,35], PBEsol as exchange–correlation functional is a revision of the PBE functional, which improves equilibrium properties of densely-packed solids and their surfaces, specifically tailored for solids. It has been shown to yield structural data in accordance with experiment reported by F. Brivio *et al*.[37]. This functional predicts the structure of common London-dispersion corrected functions without the addition of an empirical potential.

References

1. Xing, G., Mathews, N. & Sun, S. *et al*. Long-range balanced electron-and hole-transport lengths in organic-inorganic $CH_3NH_3PbI_3$. *Science* **342**, 344 (2013).
2. Im, J. H., Jang, I. H. & Pellet, N. *et al*. Growth of $CH_3NH_3PbI_3$ cuboids with controlled size for high-efficiency perovskite solar cells. *Nature nanotechnology* **9**, 927 (2014).
3. Kim, H. S. & Park, N. G. Parameters affecting I-V hysteresis of $CH_3NH_3PbI_3$ perovskite solar cells: effects of perovskite crystal size and mesoporous TiO_2 layer. *The journal of physical chemistry letters* **5**, 2927 (2014).
4. Kim, H. S., Lee, J. W. & Yantara, N. *et al*. High efficiency solid-state sensitized solar cell-based on submicrometer rutile TiO_2 nanorod and $CH_3NH_3PbI_3$ perovskite sensitizer. *Nano letters* **13**, 2412 (2013).
5. Lindblad, R., Bi, D. & Park, B. *et al*. Electronic structure of $TiO_2/CH_3NH_3PbI_3$ perovskite solar cell interfaces[J]. *The journal of physical chemistry letters, 2014* **5**, 648 (2014).
6. Xie, F. X., Zhang, D. & Su, H. *et al*. Vacuum-assisted thermal annealing of $CH_3NH_3PbI_3$ for highly stable and efficient perovskite solar cells. *ACS nano* **9**, 639 (2015).
7. Yang, Z., Surrente, A. & Galkowski, K. *et al*. Unraveling the Exciton Binding Energy and the Dielectric Constant in Single-Crystal Methylammonium Lead Triiodide Perovskite. *The Journal of Physical Chemistry Letters* **8**, 1851 (2017).
8. Albero, J., Asiri, A. M. & García, H. Influence of the composition of hybrid perovskites on their performance in solar cells. *Journal of Materials Chemistry A* **4**, 4353 (2016).
9. Tress W. Maximum Efficiency and Open-Circuit Voltage of Perovskite Solar Cells[M]//Organic-Inorganic Halide Perovskite Photovoltaics. *Springer International Publishing*, 53–77 (2016).
10. Amat, A., Mosconi, E. & Ronca, E. *et al*. Cation-induced band-gap tuning in organohalide perovskites: interplay of spin–orbit coupling and octahedra tilting. *Nano letters* **14**, 3608 (2014).
11. Hao, F., Stoumpos, C. C. & Chang, R. P. H. *et al*. Anomalous band gap behavior in mixed Sn and Pb perovskites enables broadening of absorption spectrum in solar cells. *Journal of the American Chemical Society* **136**, 8094 (2014).
12. Wehrenfennig, C., Liu, M. & Snaith, H. J. *et al*. Homogeneous Emission Line Broadening in the Organo Lead Halide Perovskite $CH_3NH_3PbI_{3-x}Cl_x$. *The journal of physical chemistry letters* **5**, 1300 (2014).
13. Li, C., Wei, J. & Sato, M. *et al*. Halide-substituted electronic properties of organometal halide perovskite films: direct and inverse photoemission studies. *ACS applied materials & interfaces* **8**, 11526 (2016).
14. Comin, R., Walters, G. & Thibau, E. S. *et al*. Structural, optical, and electronic studies of wide-bandgap lead halide perovskites. *Journal of Materials Chemistry C* **3**, 8839 (2015).
15. Ke, X., Yan, J. & Zhang, A. *et al*. Optical band gap transition from direct to indirect induced by organic content of $CH_3NH_3PbI_3$ perovskite films. *Applied Physics Letters* **107**, 091904 (2015).
16. Dittrich, T., Awino, C. & Prajongtat, P. *et al*. Temperature dependence of the band gap of $CH_3NH_3PbI_3$ stabilized with PMMA: a modulated surface photovoltage study. *The Journal of Physical Chemistry C* **119**, 23968 (2015).
17. Zhao, C., Huang, D. & Chen, J. *et al*. First-principle study for influence of an external electric field on the electronic structure and optical properties of TiO_2. *RSC Advances* **6**, 98908 (2016).
18. Varignon, J., Bristowe, N. C. & Ghosez, P. Electric field control of Jahn-Teller distortions in bulk perovskites. *Physical review letters* **116**, 057602 (2016).

19. Bellaiche, L., García, A. & Vanderbilt, D. Electric-field induced polarization paths in $Pb(Zr_{1-x}Ti_x)O_3$ alloys. *Physical Review B* **64**, 060103 (2001).
20. Xu, Y., Hong, W. & Feng, Y. *et al.* Antiferroelectricity induced by electric field in $NaNbO_3$-based lead-free ceramics. *Applied physics letters* **104**, 052903 (2014).
21. Poglitsch, A. & Weber, D. Dynamic disorder in methylammoniumtrihalogenoplumbates (II) observed by millimeter-wave spectroscopy. *The Journal of chemical physics* **87**, 6373 (1987).
22. Leppert, L., Reyes-Lillo, S. E. & Neaton, J. B. Electric Field-and Strain-Induced Rashba Effect in Hybrid Halide Perovskites. *The journal of physical chemistry letters* **7**, 3683 (2016).
23. Perdew, J. P., Burke, K. & Ernzerhof, M. Generalized gradient approximation made simple. *Physical review letters* **77**, 3865 (1996).
24. Perdew, J. P., Ruzsinszky, A. & Csonka, G. I. *et al.* Restoring the density-gradient expansion for exchange in solids and surfaces. *Physical Review Letters* **100**, 136406 (2008).
25. Menéndez-Proupin, E., Palacios, P. & Wahnón, P. *et al.* Self-consistent relativistic band structure of the $CH_3NH_3PbI_3$ perovskite. *Physical Review B* **90**, 045207 (2014).
26. Ji, D. H., Xiao, X. J. & Zhang, C. M. *et al.* Regulatory band gap of vacancy at the B sites in $CH_3NH_3Pb_{1-x}I_3$ perovskite. *Modern Physics Letters B* **30**, 1650294 (2016).
27. Guo, Y., Roy, S. & Ali, N. *et al.* Magnetic and electronic transport properties of $Yb_xCa_{1-x}MnO_3$ compounds. *Journal of applied physics* **91**, 7394 (2002).
28. Pazoki, M., Jacobsson, T. J. & Kullgren, J. *et al.* Photoinduced stark effects and mechanism of ion displacement in perovskite solar cell materials. *ACS nano* **11**, 2823 (2017).
29. Partridge, B. & Page, L. 3K: The Cosmic Microwave Background Radiation. *Annales Henri Poincaré* **49**, 62–63 (1996).
30. Li, S. D., Wang, X. Y. & Zhang, W. J. *et al.* The effect of external electric field on the performance of perovskite solar cells. *Organic Electronics* **18**, 107 (2015).
31. Hsu, P. J., Kubetzka, A. & Finco, A. *et al.* Electric-field-driven switching of individual magnetic skyrmions. *Nature nanotechnology* **12**, 123 (2017).
32. Qin, G., Qin, Z. & Yue, S. Y. *et al.* External electric field driving the ultra-low thermal conductivity of silicene. *Nanoscale* **9**, 7227 (2017).
33. Milman, V., Winkler, B. & White, J. A. *et al.* Electronic structure, properties, and phase stability of inorganic crystals: A pseudopotential plane-wave study. *International Journal of Quantum Chemistry* **77**, 895 (2000).
34. Ong, K. P., Goh, T. W. & Xu, Q. *et al.* Mechanical origin of the structural phase transition in methylammonium lead iodide $CH_3NH_3PbI_3$. *The journal of physical chemistry letters* **6**, 681 (2015).
35. Walsh, A., Scanlon, D. O. & Chen, S. *et al.* Self-Regulation Mechanism for Charged Point Defects in Hybrid Halide Perovskites. *Angewandte Chemie International Edition* **54**, 1791 (2015).
36. Umari, P., Mosconi, E. & De Angelis, F. Relativistic GW calculations on $CH_3NH_3PbI_3$ and $CH_3NH_3SnI_3$ perovskites for solar cell applications. *Scientific reports* **4**, 4467 (2014).
37. Brivio, F., Walker, A. B. & Walsh, A. Structural and electronic properties of hybrid perovskites for high-efficiency thin-film photovoltaics from first-principles. *APL Materials* **1**, 042111 (2013).

Acknowledgements

This work was supported by Joint Funds of Department of Science and Technology of Guizhou Province, LiuPanshui Administration of Science and Technology and LiuPanshui Normal University under Contract No.LH[2014]7449 and LH[2014]7456, Research Foundation for Advanced Talents of LiuPanshui Normal University (Grant No. LPSSYKYJJ201404), the Key Project of the Education Department of Guizhou Province (No. KY2015379), the National Science Foundation of China under Contract 11504078, the MIT Creative Team of Liupanshui Normal University No. LPSSYKJTD201402, the Physical Electronic Key Discipline of Guizhou Province No. ZDXK201535, the Outstanding Young Scientist Cultivation Program of Guizhou Province No. 201522.

Author Contributions

Denghui Ji designed and conducted all the calculations, and wrote the paper. Mula Na prepared the figures 1, 2 and 3, Shuling Wang, and Hong Zhang prepared the Figures 4, 5, 6, 7, 8, 9, 10, 11 and 12. Kun Zhu and Congmin Zhang analysed the data. Xiuling Li prepared the Tables. All the authors commented on the manuscript.

Additional Information

Competing Interests: The authors declare no competing interests.

Publisher's note: Springer Nature remains neutral with regard to jurisdictional claims in published maps and institutional affiliations.